

# Measuring the shear strength ratio of glued joints within the same specimen

B. Pizzo, P. Lavisci, C. Misani, P. Triboulot, N. Macchioni

**Abstract** Measuring the shear strength of both the glue-line and the solid wood with the same test specimen offers the advantages that the comparison is direct and the influence of wood variability is minimized. A new specimen geometry was developed for this purpose, and the test is run with two successive loading steps. Finite element modelling showed that the stress distribution is not significantly influencing the results, whereas the compressive pre-stress on the wood adherents results in a slightly lower resistance, probably mainly caused by micro-cracks that are already present or occur during the first loading step and propagate during the second. The analysis of fracture propagation in mode I revealed that different spruce wood batches have a much different behaviour. The method will be proposed as a standard test for epoxy adhesives used in thick joints. The evaluation criterion developed might be interesting also for other types of structural adhesives.

## Messen des Scherfestigkeitsverhältnisses verklebter Brettverbindungen innerhalb der gleichen Holzart

**Zusammenfassung** Die Scherfestigkeit sowohl von Klebefugen als auch von Vollholz an gleichen Testproben zu messen, bietet den Vorteil, dass der Vergleich direkt und der Einfluss der Holzvariabilität minimiert ist. Eine neue Holzprobengeometrie wurde zu diesem Zweck entwickelt. Der Test erfolgt mit zwei aufeinanderfolgenden Belastungsschritten. Die FEM-Berechnung zeigte, dass die Spannungsverteilung die Ergebnisse nicht wesentlich

beeinflusst, wohinegen die Druckvorspannung auf die Holzklebstoffe in einem leicht geringeren Widerstand resultiert, möglicherweise durch Mikrorisse verursacht, die schon vorhanden sind, oder beim ersten Belastungsschritt auftreten und sich durch den zweiten fortsetzen. Die Analyse der Risserweiterung in Modus I zeigt, dass unterschiedliche Fichtensortimente ein völlig unterschiedliches Verhalten aufweisen. Diese Methode wird als Standardtest für Epoxidharze für dicke Brettverbindungen vorgeschlagen. Das entwickelte Bewertungskriterium könnte auch für andere Arten von Konstruktionsklebern interessant sein.

## 1 Introduction

Shear strength is the reference parameter for the evaluation of adhesive bonds, because it is the most common interfacial stress under service conditions. It also provides an useful criterion for the estimation of the mechanical compatibility between wood and adhesive (Pizzo et al. 2003): the direct comparison of bondline shear strength with the actual wood shear strength measured on the same batch. This is likely to become an useful evaluation criterion for every type of wood adhesive.

Using the compressive shear specimen described by Lavisci et al. (2001), the average shear strength of spruce (*Picea abies* L.) solid wood, measured on more than 150 specimens cut from different batches, is  $\tau_{SW}=8.2$  MPa (CV=17%). Values range between 4 MPa and 14 MPa (95% of the values are comprised between 5 MPa and 10.5 MPa). This variability is very high, and penalizing if the  $\tau_{SW}$  is used in a standard specification or for design calculations. Limiting the comparison to specimens cut from the same batch of wood would reduce the influence of variability, but also the applicability of the results. Although no specific literature references were found, an useful approach seemed to be the measurement of both parameters directly on each single glued joint specimen. The objective of this paper is to report about the development of such a test specimen and to analyse its reliability and applicability as a laboratory test for the characterisation of structural wood adhesives.

## 2 Materials and methods

A new geometry was developed for the compressive shear specimen (Fig. 1), adding two 10×10 mm grooves on each face opposed to the load application, in order to test the

Published online: 9 July 2003

B. Pizzo (✉)  
Istituto per la Valorizzazione del Legno e delle Specie Arboree (CNR), Via Madonna del Piano, I-50019 Sesto Fiorentino (FI), Italy  
E-mail: b.pizzo@ivalsa.cnr.it

P. Lavisci  
LegnoDOC srl, Via de' Bernardi 64, I-50145 Firenze, Italy

C. Misani  
Mapei spa, Via Cafiero 22, I-20158 Milano, Italy

P. Triboulot  
LERMAB-UMR INRA/ENGREF/UHP-ENSTIB N°1093,  
Equipe Génie Civil Bois, 27, rue du Merle Blanc,  
F-88051 Epinal, France

N. Macchioni  
Istituto per la Ricerca sul Legno (CNR),  
Via Barazzuoli 23, I-50136 Firenze, Italy

We especially thank Simona Lazzeri for the SEM micrographies and Nicola Franchini for the FEM analysis.

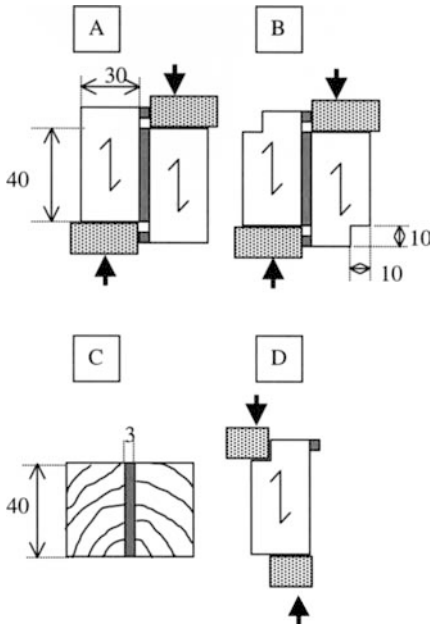


**Fig. 1.** Geometry of glued joint specimens with a single groove (A) as described in Lavisci et al. (2001), or with a double groove (B) as developed for the present work. The cross section in the sheared area is equivalent for both specimens (C). In the specimen with a double groove a second test is possible, where one of the solid wood adherents from a broken glued joint specimen (D) is loaded without any offset

**Abb. 1.** Geometrie von Prüfkörpern von Klebeverbindungen mit einer einzelnen Kerbe (A) wie bei Lavisci et al. (2001) beschrieben oder mit einer Doppelkerbe (B) wie in vorliegender Arbeit entwickelt. Der Querschnitt in der Scherregion ist für beide Proben äquivalent (C). In der Probe mit einer Doppelkerbe ist ein zweiter Test möglich, in dem einer der Massivholzteile einer gebrochenen Klebefugenprobe (D) ohne Vorlauf belastet wird

glueline in a first loading step and the solid wood in a second loading step. The effects of introducing the grooves in the test specimens were analysed with a Finite Element Model (FEM), with the comparison of the shear strengths measured under different loading conditions and with the study of the crack propagation in the solid wood.

## 2.1 Model

In order to check the differences in stress distribution, a finite element model of the specimen has been analysed. The model was built and analysed with a commercial software, where both the wood and the adhesives are considered ideal elastic bodies. The two specimen geometries were represented with a three-dimensional network of cubic cells (*brick 8 nodes*) with a 2.5 mm side. The offset was modelled with four lines of cells with 0.75 mm depth, assigning them the elastic parameters of spruce for wood specimens and those of the adhesive for glued specimens (Fig. 4). The following values were assigned to spruce wood, based on 0.43 g/cm<sup>3</sup> density (Guitard 1987):  $E_I = E_y = 13800$  MPa;  $E_r = E_x = 910$  MPa;  $E_t = E_z = 490$  MPa;  $\nu_{LR} = \nu_{yx} = 0.454$ ;  $\nu_{TL} = \nu_{zy} = 0.019$ ;  $\nu_{RT} = \nu_{xz} = 0.558$ .

Shear modules were automatically calculated by the software on the base of the above elastic parameters. The presence of growth rings and their inclination with respect to the shear plane was not considered, so the results are

valid only for the comparison between specimen geometries. The following elastic parameters have been assigned to the glueline, typical of a structural epoxy-based adhesives for on-site applications:

$$E = E_x = E_y = E_z = 6000 \text{ MPa}; \nu = 0.3.$$

Loading was modeled as distributed by a steel plate, with the specimen simply supported by it.

## 2.2

### Comparison of shear strength

Each specimen was tested twice in shear by compression loading:

- the first loading step is at the wood-adhesive interface (Fig. 1B), with an offset equal to the adhesive's thickness (3 mm in our case);
- the second loading step is performed on solid wood, on one of the two adherents, without any offset (Fig. 1D). Preferably, the side where the fracture progressed during the first loading step is chosen, because its wood shear strength should be lower than on the other side. ISO 8905 requires an offset of 3 mm to account for eventual grain deviations: Okkonen and River (1988) observed, that this offset lowers wood's shear strength, as confirmed by some preliminary tests for spruce wood.

The new testing procedure introduces two major differences with respect to the traditional ones:

1. the adherents are subjected twice to mechanical stress, so it is possible that the first stress has an influence on the result of the second loading step (e.g. if it is higher than the proportional limit and/or if it produces micro-cracks);
2. the stress distribution is different in the two loading steps: in particular, the offset in the first loading step produces a moment which is balanced by tension stresses in a direction perpendicular to the grain.

In order to compare the shear strength values obtained using the new specimen geometry and the ISO 8905 geometry, solid wood specimens were prepared with spruce wood from six different batches (Table 1), at different angles of the growth rings to the shear plane. Testing was done as for glued joint specimens, with constant load application (0.1 MPa/sec): a first loading in the central area of the specimen (with offset, Fig. 1B), followed by a second loading on one of the sides (without offset, Fig. 1D). At least 10 useful results were considered for each sample. Moreover, with wood from batch A2 a series of "twin" specimens was prepared (Fig. 2) in order to run a loading step with the ISO 8905 geometry, without any pre-stress.

## 2.3

### Fracture energy

The early approaches on applications of the fracture mechanics to wood were of linear type (LEFM, *Linear Elastic Fracture Mechanics*). This approach gave good results in the study of the solid wood (Triboulot et al.

**Table 1.** The 6 batches of spruce wood, used for the comparison of shear strength between the new specimen geometry and the ISO 8905 geometry, in standard atmosphere [20/65], are reported (standard deviations in brackets)

**Tabelle 1.** Die sechs Fichtenholzstapel, die für den Vergleich der Scherfestigkeit zwischen der neuen Probengeometrie und der ISO 8905 Geometrie verwendet wurden, wurden in unterschiedlichen Jahrring-Winkeln zur Scherebene geschnitten. Die Durchschnittsdichte und die kompressive Festigkeit der sechs Stapel in Standard-Atmosphäre [20/65] wird angegeben (Standardabweichungen in Klammern)

Batch	A1	A2	A3	A4	A5	A6
Density (g/cm <sup>3</sup> ) ISO 3131	0.433 (±0.007)	0.401 (±0.004)	0.457 (±0.005)	0.380 (±0.004)	0.358 (±0.005)	0.414 (±0.006)
Compressive strength (Mpa) ISO 3787	45.6 (±1.1)	41.7 (±0.9)	46.7 (±0.5)	38.5 (±1.1)	36.3 (±0.6)	44.6 (±0.9)
Angle of shear specimens	20° 90°	30°	20°	90°	90°	45° 90°

1983—Triboulot et al. 1984) and also it has been successfully applied to the glued joints (Duchanois 1984). Nevertheless, the behaviour of the fracture curves presents a non-linear part, that can be important in our case. Boström (1994a) suggests that elastic linear analysis in wood is limited in application when there is not an initial crack or when the surface of propagation of the fracture is large in relation to the thickness of the specimen, or in relation to the length of the cracks. For this reason, he proposes a different type of analysis. This elasto-plastic analysis has been chosen by others authors. Daudeville (1999) compared the two approaches for the specimen suggested as a standard by the RILEM and the CIB-W18 (Larsen and Gustafsson 1989): he noticed that the plastic part of the curves is important and that the linear elastic analysis is not adapted to this type of specimen. Also Stanzl-Tschegg et al. (1994–1995), Tan et al. (1995) and Reiterer et al. (2000) chose the elasto-plastic analysis for their tests. The fracture energy in mode I was measured for 2 different angles of the growth rings to the fracture plane (Table 2). Because of material availability, it was possible to obtain specimens only for 5 batches. The “compact type tension (CT)” specimen proposed by Boström (1994b) was used (Fig. 3), and the fracture notch was obtained with a razor blade. The specific fracture energy  $G_f$  was calculated from the load-displacement curves as:

$$G_f = \frac{1}{BW} \int F(u) du$$

where  $u$  is the displacement of the crosshead during the test (mm);  $F$  is the load (N);  $B$  and  $W$  are, respectively, the width and the length of the fracture surface, in mm. Tests were run on an Instron model 4411, with a 1000 N load cell (0.5% accuracy), displacement being measured by the machine’s internal transducer. The crosshead speed was fixed at 1 mm/min.

### 3 Results and discussion

The finite element model indicated that at the load of 15 kN (an average rupture value for glued specimens tested dry, without any accelerated ageing) significant tension perpendicular to the grain is present at the upper and lower borders of the shear plane. However, the stress distribution at the wood-adhesive interface does not

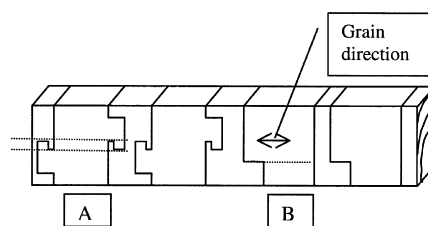


**Fig. 2.** Specimens with offset (A) and without offset (B) cut in “twin” series from the same bar of spruce solid wood (batch A2)  
**Abb. 2.** Proben mit Offset (A) und ohne Offset (B) in Zwillingsreihen von den gleichen Fichtenmassivholz-Balken geschnitten

**Table 2.** Samples for the fracture testing in mode I, cut from five batches of spruce wood and with different angles of growth rings to the fracture plane

**Tabelle 2.** Proben für den Bruchtest in Modus I, geschnitten aus fünf Fichtenholzstapeln mit unterschiedlichen Jahrring-Winkeln zur Bruchebene

Batch	A1	A2	A4	A5	A6
Angle	25° 75°	20° 55°	85° 35°	90° 45°	80° 45° 85°

significantly differ between the two geometries, but a large portion of the adherent is in compression with stresses in the range of 5–10 MPa (peak stress is 17 MPa).

Therefore, the fracture in the shear plane is started by tension stress at the borders, as confirmed by SEM observations of fracture surfaces (Figs. 5 and 6), and the compressive stress in the bulk of the adherent may be significantly high to produce micro-cracks that will eventually influence the result of the second loading step (aimed at measuring  $\tau_{SW}$ ). This possibility, which is related only to wood characteristics, was analysed by comparing the shear strengths of solid wood (Fig. 7). Results show a general trend to a lower resistance in the second loading step (no offset, pre-stressed) with respect to the first loading step, even if statistic significance at 99% confidence is present only for batches A2, A3 and A6-90°. Only batch A6 tested at 45° shows an opposite trend, but the average values are not statistically different. For our samples, shear strength is neither correlated with wood density ( $R^2=0.55$ ) nor with compressive strength ( $R^2=0.42$ ).

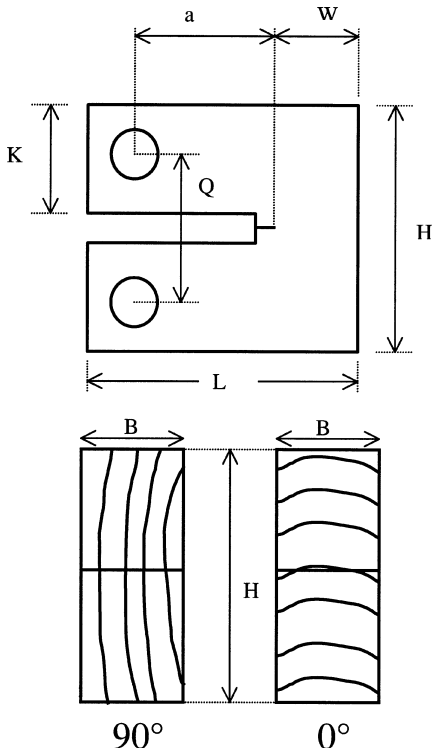


**Fig. 3.** Specimen for the measurement of fracture energy in mode I of solid wood (Boström 1994a). The angle of growth rings to the fracture plane may vary from  $0^\circ$  (radial test) to  $90^\circ$  (tangential test). Dimensions:  $a+W=5$  cm;  $a/W=0.61$ ;  $H=6$  cm;  $L=6.5$  cm;  $B=3$  cm

**Abb. 3.** Proben zur Messung der Bruchenergie von Vollholz in Modus I (Boström 1994a). Der Jahrring-Winkel zur Bruchebene kann von  $0^\circ$  (radialer Test) bis zu  $90^\circ$  (tangentialer Test) variieren. Dimensionen:  $a+W=5$  cm;  $a/W=0.61$ ;  $H=6$  cm;  $L=6.5$  cm;  $B=3$  cm

The average shear strength of solid wood is, for the new specimen geometry,  $\tau_{SW}=8$  MPa (CV 6.5%), which compares favorably with the results obtained using the old geometry ( $\tau_{SW}=8.2$  MPa; CV=17%). The coefficients of variation of single batches are low in the second test (2.7–7%), with the exception of A6- $90^\circ$  (10%). The fracture plane propagates in the earlywood at angles  $<45^\circ$ , as observed also for the glued specimens. For batch A2, where the difference is statistically significant, the series of “twin” specimens where all loaded without any pre-stress. Results (Fig. 8) show in this case no difference, confirming our hypothesis that micro-cracks developed during the first loading step may be the reason for a lower shear strength in the second loading step, although no evidence of such micro-fractures was found at the SEM observation. The possibility that a stress combination of tension perpendicular to the grain and compression along the grain produces micro-cracks was postulated also by Tan et al. (1995). We supposed that the various batches may have a different ability to resist to the propagation of these micro-cracks, an for this reason their fracture behavior in mode I was analysed. The load-displacement curves are very reproducible within samples (same batch and angle) and the fracture propagates in a stable way in all the cases, confirming that the specimen geometry was well calibrated (Fig. 9). The fracture energy  $G_f$  gives a quantitative

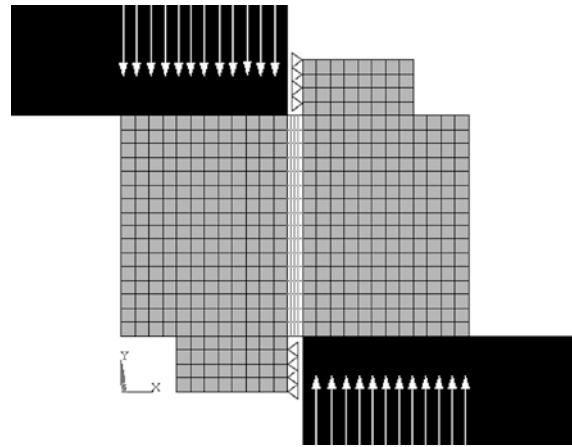


**Fig. 4.** Diagram of the finite element model developed for the analysis of the stress distribution of specimen geometries. The same model has been used both for the glued specimens and for the solid wood ones. The cells are distributed as follows: Black = steel blocks for the application of the load; Grey = wood; White = adhesive in the glued specimens/wood in the solid wood specimens. The small pieces of adhesive (or solid wood), that constitute the vertical supports of specimens when placed in the test jig, are modelled with carriers that permit the movement along the direction of application of the load

**Abb. 4.** Diagramm des FEM-Modells für die Analyse der Spannungsverteilung der Probengeometrie entwickelt. Das gleiche Modell wurde sowohl für die Kleberproben als auch für die Massivholzproben verwendet. Die Zellen werden folgendermaßen verteilt: schwarz = Stahlblöcke für die Einleitung der Last; grau = Holz; weiß = Kleber in den verklebten Proben/Holz bei Massivholzproben. Die kleinen Kleberteile (oder Massivholz), die die vertikale Unterstützung der Proben im Testgerät darstellen, werden mit Trägern versehen, die die Bewegung entlang der Richtung der Spannungsanwendung erlauben

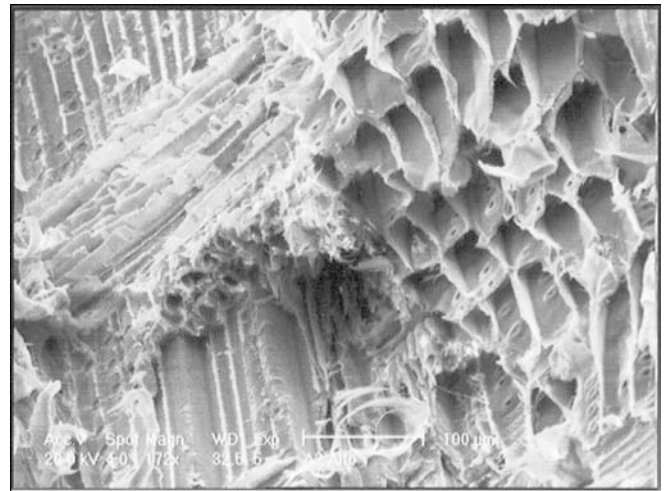


**Fig. 5.** Example of fracture surface for the upper border of the shear plane in batch A2, tested with offset (first test). Many fibers in both the earlywood and the latewood show the transversal rupture typical of traction perpendicular to the grain

**Abb. 5.** Ein Beispiel der Bruchoberfläche für den oberen Rand der Scherebene in Stapel A2, mittels Offset getestet (erster Test). Sowohl bei Frühholz als auch bei Spätholz zeigen die Fasern transversal Einrisse charakteristisch für Zugbeanspruchung senkrecht zur Faser

indication of the easiness of propagation of existing fractures and results (Fig. 10) show the greatest differences for the largest angles of growth rings to the fracture plane

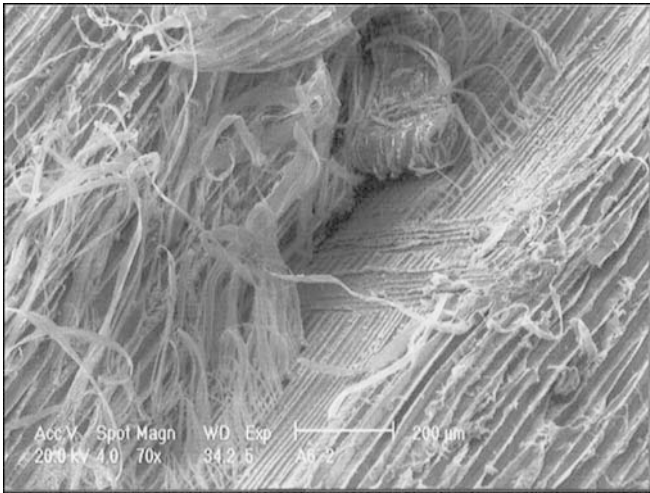


**Fig. 6.** The “fuzzy” aspect typical of a shear fracture, normally present on the central and largest part of the shear plane  
**Abb. 6.** Das für einen Scherbruch charakteristische ausgefranste Erscheinungsbild, das gewöhnlich auf dem zentralen und größten Teil der Scherebene vorhanden ist

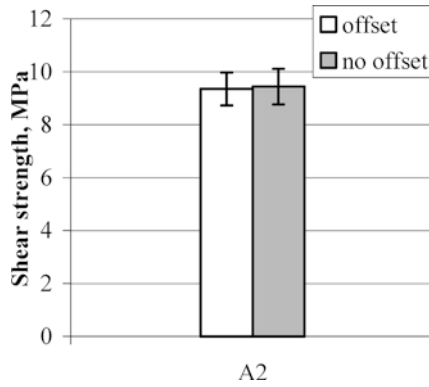


**Fig. 8.** Shear strength of “twin” specimens from batch A2, loaded without any pre-stress. Vertical bars show 99% confidence intervals  
**Abb. 8.** Scherfestigkeit von Zwillingssproben des Stapel A2, ohne jegliche Vorspannung belastet. Vertikale Balken zeigen 99% Vertrauensintervalle

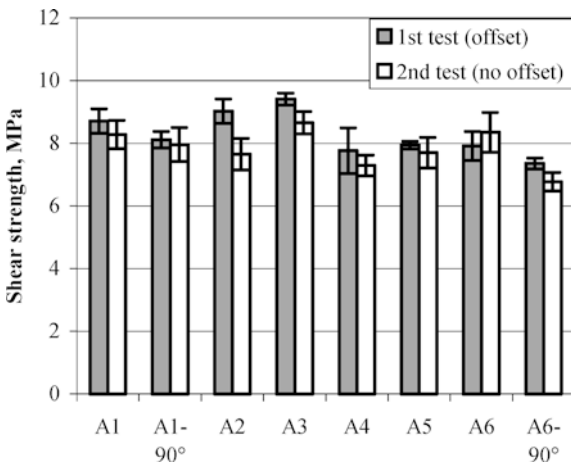


**Fig. 7.** Results of the shear tests on solid wood specimens, for different batches of spruce wood. Vertical bars show 99% confidence intervals  
**Abb. 7.** Ergebnisse der Schertests von Massivholzproben, unterschiedlicher Fichtenholzstapel. Vertikale Balken zeigen 99% Vertrauensintervalle

(tangential test, at 90°). Values range from 137 to 316 J/m<sup>2</sup>, in according to results from Stanzl-Tschegg et al. (1994, 1995) that found values from 170 to 315 J/m<sup>2</sup> for spruce wood with different drying treatments, and Reiterer et al. (2000) that report a value of 260 J/m<sup>2</sup> for spruce in the RL configuration (in our case, a 0° angle). Boström (1994a) found higher values (445–595 J/m<sup>2</sup>), and Daudeville (1999) lower ones (157 et 251 J/m<sup>2</sup>). Significantly, Stanzl-Tschegg et al. (1995) found higher fracture energies in the RL configuration (0° angle) than in the TL configuration (90° angle): we had this trend for four batches, but an opposite trend for batch A1. Based on the load-displacement curves, other parameters have been calculated in order to have a different view of the results. The tensile stress at which

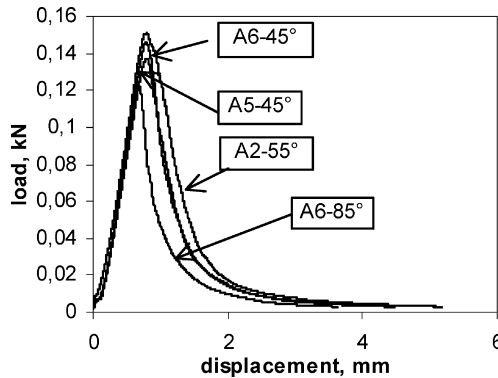


**Fig. 9.** The shape of the load-displacement curves is very similar between batches, mainly in the first part of the curve. The second part (plastic behavior) is where the differences between batches are apparent  
**Abb. 9.** Der Verlauf der Spannungsdeformationskurven ist zwischen den Stapeln sehr ähnlich, vor allem im ersten Teil der Kurve. Der zweite Teil (plastisches Verhalten) tritt auf bei offensichtlich unterschiedlichen Stapeln

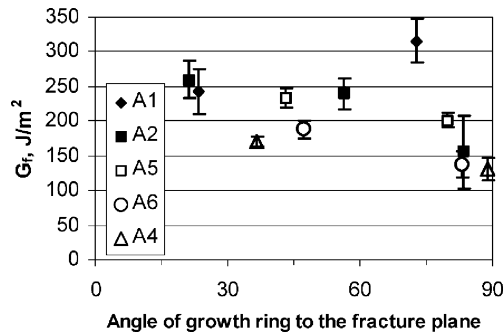


**Fig. 10.** Fracture energy versus the angle of growth ring to the fracture plane, for different batches of spruce wood. Vertical bars show 99% confidence intervals  
**Abb. 10.** Bruchenergie versus Jahrring-Winkel zur Bruchebene für unterschiedliche Massivholzstapel. Vertikale Balken zeigen 99% Vertrauensintervalle

fracture propagates  $\sigma_{int}$  has been calculated, for our specimens, according to the equation proposed by Reiterer et al. (2000):

$$\sigma_{int} = \frac{F}{WB} + \frac{M}{R} = YF$$

where  $F$  is the maximum load obtained in the test (N);  $W$  and  $B$  are the dimensions of the resisting surface;  $M$  is the bending moment at the maximum load, and  $R$  is the moment of resistance (depending on the geometry of the specimen). In our case, the geometric constant  $Y$  has a value of  $2.83 \times 10^{-2} \text{ mm}^{-2}$ . The  $\sigma_{int}$  is not very sensible to differences between batches, and has a general trend of diminishing with the higher angles of growth rings to the fracture plane (Fig. 11). This is consistent with the fact that in the  $90^\circ$  test the parenchyma rays are in the fracture plane. Values similar to ours were found by Boström (1994b) with a similar specimen, whereas Reiterer et al. (2000) found lower values with a different specimen type. Since the load-displacement curves of the different batches have a very similar shape (Fig. 9), the two parameters  $G_f$  and  $\sigma_{int}$  may be used to calculate a normalized fracture energy,  $G_{f, Norm}$ , that we defined as follows:

$$G_{f, Norm} = \frac{G_f}{\sigma_{int}}$$

This parameter, not physically measurable, has the dimensions of length and represents the fracture energy required for unit stress of crack propagation. High values of  $G_{f, Norm}$  describe a material in which fracture starts easily but propagates with much energy, while a low value indicates a more brittle material. Results expressed in terms of  $G_{f, Norm}$  are reported in Fig. 12. This parameter is very sensitive to the differences between batches of spruce wood: it grows with the angle for A1 and A2, is stable for A5 and decreases for A6 and A4. A similar parameter which is frequently used in fracture mechanics is the characteristic length,  $L_{ch}$ , that considers also the effective modulus of the material,  $E_{eff}$  as:

$$L_{ch} = \frac{G_f E_{eff}}{\sigma_{int}^2}$$

Also in this case a lower value indicates a higher brittleness. We defined  $E_{eff}$  as the ratio of the tensile stress  $\sigma_{int}$  to the effective deformation  $\epsilon_{eff}$  as follows:

$$E_{eff} = \frac{\sigma_{int}}{\epsilon_{eff}}$$

and therefore  $\epsilon_{eff}$ , for our test conditions, is:

$$\epsilon_{eff} = \frac{\Delta u}{\sigma}$$

where  $\Delta u$  is the measured displacement, and  $Q$  is the distance between the loading holes in the specimen, which is taken as the reference length. Because  $\sigma_{int}$  may be expressed as:

$$\sigma_{int} = FY$$

then  $E_{eff}$  may be expressed as:

$$E_{eff} = \frac{FYQ}{\Delta u} = \frac{F}{\Delta u} YQ$$

In this case, the ratio  $\frac{F}{\Delta u}$  is the slope of the elastic portion of the load-displacement curve. We used the portion of the curves comprised between 30% and 80% of the maximum load to calculate  $E_{eff}$  for each specimen, and Fig. 13 reports the average values of each batch. The results from fracture tests expressed in terms of

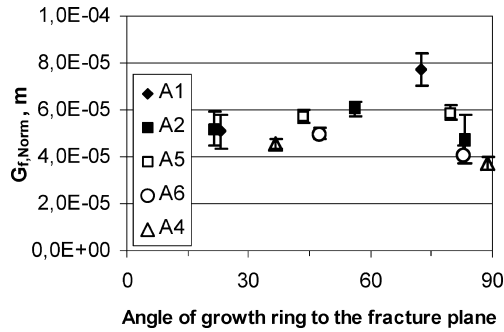


Fig. 12. Normalized fracture energy versus the angle of growth rings to the fracture plane, for different batches of spruce wood. Vertical bars show 99% confidence intervals  
Abb. 12. Normalisierte Bruchenergie versus Jahring-Winkel zur Bruchebene für unterschiedliche Fichtenholzstapel. Vertikale Balken zeigen 99% Vertrauensintervalle

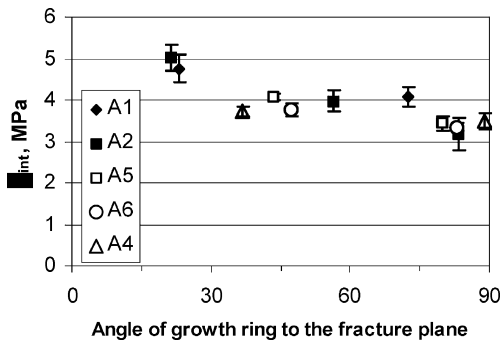


Fig. 11. Stress of crack propagation versus the angle of growth rings to the fracture plane, for different batches of spruce wood. Vertical bars show 99% confidence intervals  
Abb. 11. Spannung der Rissausbreitung versus Jahring-Winkel zur Bruchebene, für unterschiedliche Fichtenholzstapel. Vertikale Balken zeigen 99% Vertrauensintervalle

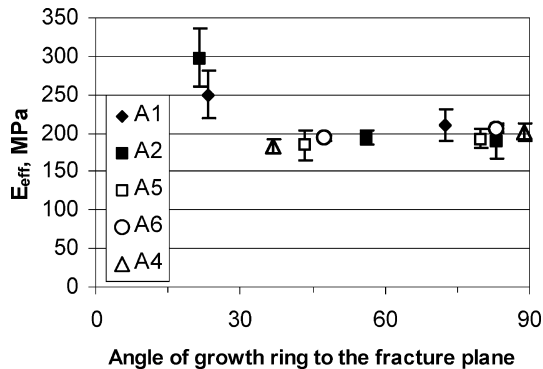


Fig. 13. Effective modulus of elasticity versus the angle of growth rings to the fracture plane, for different batches of spruce wood. Vertical bars show 99% confidence intervals  
Abb. 13. Effektiver Elastizitätsmodulus versus Jahring-Winkel zur Bruchebene für unterschiedliche Fichtenholzstapel. Vertikale Balken zeigen 99% Vertrauensintervalle

characteristic length,  $L_{ch}$ , are reported in Fig. 14.  $E_{eff}$  is significantly higher, but not much different between batches for angles  $<30^\circ$ , and remains quite constant at angles  $>30^\circ$ : it is just a result of the test geometry and seems to have a minor influence on the results. The  $L_{ch}$  shows a trend of growth with the angle for batches A1 and A5, is quite stable for A2 and decreases for A6 and A4. Therefore,  $G_{f, Norm}$  and  $L_{ch}$  give different indications for batches A2 and A5. Batch A6 and A4 have much lower values than other batches, for both parameters, at the high angle of growth rings to the fracture plane. The reason for this difference has been researched in wood anatomy: for all batches, the fracture tends to propagate in the tangential direction within the earlywood and to cross the latewood in the radial direction, and this fracture pattern has already been observed by Tan et al. (1995). The propagation in the tangential direction is made possible by intra-cellular rupture, in the longitudinal direction, of the thin walls; the propagation in the radial direction, across the thick latewood walls, is normally inter-cellular and follows the direction of rays (Fig. 15). The tracheid lumen diameter in the latewood may influence this pattern, as well as the thickness of tracheid walls and the relative thickness of earlywood and latewood within the growth ring. The relative influence of the different anatomic features is being thoroughly analysed and will be reported separately. According to the fracture pattern observed, tests at higher angles ( $45^\circ$ – $90^\circ$ ) should have higher normalized fracture energies ( $G_{f, Norm}$ ), therefore batches A6 and A4 are an exception to this rule. In fact, all the batches except A6 and A4 have a pronounced waviness in the fracture surfaces obtained at higher angles (Fig. 16), which also indicates a different energy consumption for fracture propagation. Considering the shear strength (Fig. 7), a comparison of batches A1 and A6 is interesting: tested at  $90^\circ$ , A1 has no statistically significant decrease between the first test and the second (in pre-stressed conditions), while A6 does have this difference. Also, A1 is more resistant in shear and stiffer in cleavage (higher  $E_{eff}$ ) than A6 in general terms, whereas A6 has the highest variability ( $CV=10\%$ ). This different shear strength is, according to our results,

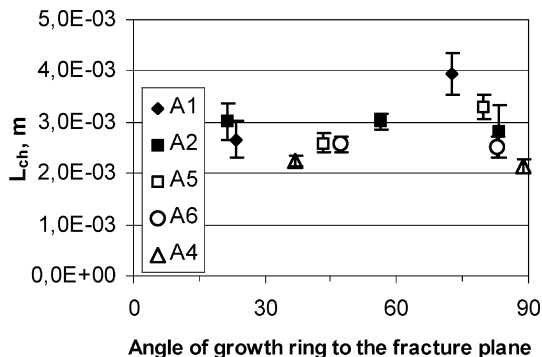


Fig. 14. Characteristic length versus the angle of growth rings to the fracture plane, for different batches of spruce wood. Vertical bars show 99% confidence intervals

Abb. 14. Charakteristische Länge versus Jahrring-Winkel zur Bruchebene für unterschiedliche Fichtenholzstapel. Vertikale Balken zeigen 99% Vertrauensintervalle

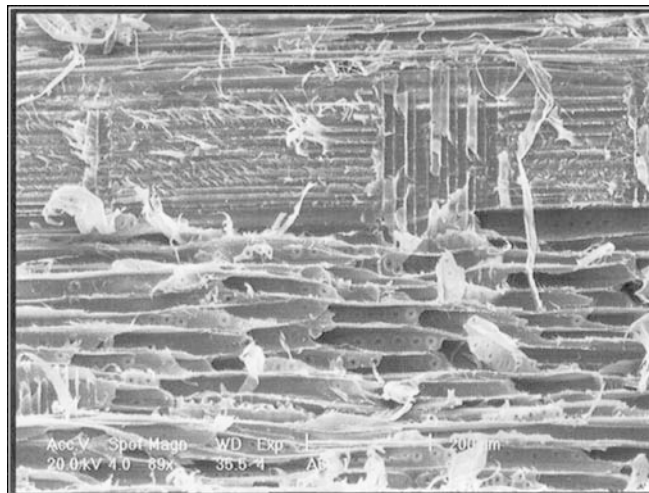


Fig. 15. Transition from the intra-cellular fracture in earlywood to the inter-cellular fracture in the latewood. Parenchyma rays constitute a preferential transition point

Abb. 15. Übergang vom intrazellulären Bruch in Frühholz zum interzellulären Bruch in Spätholz. Parenchym-Strahlen stellen einen bevorzugten Übertragungspunkt dar

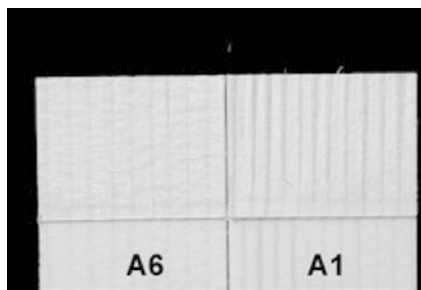


Fig. 16. Comparison of the fracture surfaces of batch A6 (left) and A1 (right), tested at the highest angles. A6 is flat whereas A1 is wavy

Abb. 16. Vergleich der Bruchoberflächen von Stapel A6 (links) und A1 (rechts), getestet bei den höchsten Winkeln. A6 ist flach, wohingegen A1 wellig ist

related to the different fracture properties of the two spruce wood batches.

#### 4

#### Conclusions

Measuring the shear strength of both the glueline and the solid wood adherents within the same test specimen offers indeed a great advantage: the comparison is really direct, the influence of wood variability is minimized and the test is quick and simple. The influence of the new specimen geometry on stress distribution is not significantly influencing the results, while the compressive pre-stress on the wood adherents results in a slightly lower resistance, which is much probably caused by micro-cracks that occur during the first loading step and propagate during the second. As expected, different spruce wood batches have shown a different fracture behaviour. Therefore, the selection of suitable wood batches for the specimen preparation may benefit from the use of a parameter that describes crack propagation: based on our results, a value

of  $G_{f, Norm} > 5 \times 10^{-5}$  m (measured between  $45^\circ$  and  $90^\circ$ , preferably as close as possible to  $90^\circ$ ) should guarantee that micro-cracks eventually present in the wood (e.g. those produced in the first loading step, but also in drying and cutting operations) do not have a significant influence on the measurement of wood shear strength. It is also necessary to underline the importance of limiting the angle of growth rings to the glue line in the range of  $45^\circ$ – $90^\circ$ , while preparing the glued specimens for shear tests. Results from this work will be proposed as a standard test method for on-site epoxy adhesives used in thick joints. But the evaluation of adhesive bonds based on the “direct” comparison of their performance with that of solid wood used in the adherents is indeed a new and useful criterion, which might be interesting also for other applications (e.g. structural adhesives as in EN 301 and non-structural adhesives as in EN 204).

## References

- Boström L** (1994a) The stress-displacement relation of wood perpendicular to the grain. Part 1: Experimental determination of the stress-displacement relation. *Wood Sci Technol* 28(4):309–317
- Boström L** (1994b) The stress-displacement relation of wood perpendicular to the grain. Part 1: Application of the Fictitious Crack Model to the Compact Tension Specimen. *Wood Sci Technol* 28(5):319–327
- Daudeville L** (1999) Fracture in spruce: experiment and numerical analysis by linear and non linear fracture mechanics. *Holz Roh-Werkstoff* 57:425–432
- Duchanois G** (1984) Mesure de la ténacité et étude du comportement mécanique des joints bois-colle. Thèse de Docteur-Ingénieur INPL, Nancy University
- Guitard D** (1987) Mécanique du matériau bois et composites. Cepadues ed.
- International Organization for Standardization** (1988) Sawn timber. Test methods. Determination of ultimate strength in shearing parallel to grain. ISO 8905
- Lavisci P, Berti S, Pizzo B, Triboulot P, Zanuttini R** (2001) A shear test for structural adhesives used in the consolidation of old timber. *Holz Roh- Werkstoff* 59(1/2):145–152
- Larsen HJ, Gustafsson PJ** (1989) Design of end-notched beams. 22th CIB W-18 A meeting. Berlin, Germany. Paper 22–10–1
- Okkonen EA, River BH** (1988) Factors affecting the strength of block-shear specimens. *Forest Prod J* 39(1):43–50
- Pizzo B, Lavisci P, Misani C, Triboulot P** (2003) The compatibility of structural adhesives with wood. (in press)
- Reiterer A, Stanzl-Tschegg SE, Tschegg EK** (2000) Mode I fracture and acoustic emission of softwood and hardwood. *Wood Sci Technol* 34:417–430
- Sih GC, Paris P, Irwin GR** (1965) On cracks in rectilinear anisotropic bodies using singular isoparametric elements. *Int J Fract Mech* 1:189–203
- Stanzl-Tschegg SE, Tschegg EK, Teischinger A** (1994) Fracture energy of spruce wood after different drying procedures. *Wood Fibre Sci* 26(4):467–478
- Stanzl-Tschegg SE, Tan DM, Tschegg EK** (1995) New splitting method for wood fracture characterization. *Wood Sci Technol* 29(1):31–50
- Tan DM, Stanzl-Tschegg SE, Tschegg EK** (1995) Models of wood fracture in Mode I and Mode II. *Holz Roh- Werkstoff* 53:159–164
- Triboulot P, Jodin P, Pluvinage G** (1982) Mesure des facteurs d'intensité de contraintes critiques et des taux de restitution d'énergie dans le bois sur éprouvettes entaillées. *Ann For Sci* 39(1):63–76
- Triboulot P, Otha M, Asano I** (1983) Application of fracture mechanics on the cutting process of wood. *Mokuzai-Gakkaishi* 29(2):111–117
- Triboulot P, Jodin P, Pluvinage G** (1984) Validity of fracture mechanics concepts applied to wood by finite element calculation. *Wood Sci Technol* 18:51–58